Peer-reviewed version available at Remote Sens. 2018, 10, 854; doi:10.3390/rs10060854

Using Multi-Spectral UAV Imagery to Extract Tree Crop Structural Properties and Assess Pruning Effects

Kasper Johansen [1]*, Tri Raharjo [2], Matthew F. McCabe [1]

[1] Water Desalination and Reuse Center, King Abdullah University of Science and Technology, Al Jazri Building West, Thuwal, 23955-6900, Kingdom of Saudi Arabia; kasper.johansen@kaust.edu.sa, matthew.mccabe@kaust.edu.sa.
[2] Ministry of Agrarian and Spatial Planning, National Land Agency, Jalan H. Agus Salim 58, Jakarta Pusat 10350, Indonesia; triraharjo.geo@gmail.com.

* Correspondence: kasper.johansen@kaust.edu.sa, +966-12-8028192

Abstract: Unmanned aerial vehicles (UAV) provide an unprecedented capacity to monitor the development and dynamics of tree growth and structure through time. It is generally thought that the pruning of tree crops encourages new growth, has a positive effect on fruiting, makes fruit-picking easier, and may increase yield, as it increases light interception and tree crown surface area. To establish the response of pruning in an orchard of lychee trees, an assessment of changes in tree structure, i.e. tree crown perimeter, width, height, area and Plant Projective Cover (PPC), was undertaken using multi-spectral UAV imagery collected before and after a pruning event. While tree crown perimeter, width and area could be derived directly from the delineated tree crowns, height was estimated from a produced canopy height model and PPC was most accurately predicted based on the NIR band. Pre- and post-pruning results showed significant differences in all measured tree structural parameters, including an average decrease in tree crown perimeter of 1.94 m, tree crown width of 0.57 m, tree crown height of 0.62 m, tree crown area of 3.5 m^2, and PPC of 14.8%. In order to provide guidance on data collection protocols for orchard management, the impact of flying height variations was also examined, offering some insight into the influence of scale and the scalability of this UAV based approach for larger orchards. The different flying heights (i.e. 30, 50 and 70 m) produced similar measurements of tree crown width and PPC, while tree crown perimeter, area and height measurements decreased with increasing flying height. Overall, these results illustrate that routine collection of multi-spectral UAV imagery can provide a means of assessing pruning effects on changes in tree structure in commercial orchards, and highlight the importance of collecting imagery with consistent flight configurations, as varying flying heights may cause changes to tree structural measurements.

Keywords: UAV; multi-spectral; lychee; pruning; tree crop structure; change detection

Peer-reviewed version available at Remote Sens. 2018, 10, 854; doi:10.3390/rs10060854

1. Introduction

In order to increase the production of any agricultural system, activities such as crop monitoring for assessing growth, stresses, pests, fertiliser, water, nutrient condition and irrigation are all required [1,2]. In addition to this, post-harvesting handling, such as tree pruning, has also been shown to be beneficial for enhancing yields [3]. Pruning includes cutting and trimming of branches, and as such it affects the structural attributes of tree crops. Pruning of fruit trees promotes new growth [4], makes manual fruit-picking easier, and increases light interception, which is important for fruit quality [5,6]. Tree pruning has also been shown to have implications for crop harvest and nutrition, pest and disease control, soil protection and irrigation strategies [7]. Increasing flowering, fruit colour, soluble solids concentrations and flower bud formation, and decreasing titratable acid content are other benefits linked to pruning of fruit trees [3,8-10].

However, tree pruning is a costly practice, especially if done using manual labour, which is usually the case for small orchards [11]. Often, tree crown reduction goals are set to optimise pruning [12], but the assessment to determine if these goals have been achieved is generally based on manual measurement or empirical models, which are time-consuming and potentially inconsistent [4]. Hence, there is a need for more efficient and consistent tree crop pruning monitoring strategies that can be applied in a consistent manner at the orchard level.

Remote sensing is ideally suited for monitoring tasks and has the benefit of providing multi-temporal information on tree structure, and changes in these, over time [13]. However, as many plantations are relatively small (1-50 ha) [8], the use of high spatial resolution satellite and airborne imagery quickly becomes cost-prohibitive [14]. The rapid development of Unmanned Aerial Vehicles (UAVs) and miniaturised sensors in the last decade is now offering an alternative to more traditional satellite and airborne based remote sensing [15,16]. This is largely due to the fact that UAVs are light-weight, low-cost, suitable for autonomous data collection, and highly deployable, allowing remotely sensed imagery to be collected at any time for smaller areas (< 1 km^2), subject to suitable weather conditions [4].

The mapping of tree structural parameters such as tree height and crown size provides key indicators for plant growth, biomass, yield, as well as for assessing pruning practices [4,17,18]. As high spatial resolution imagery is required for assessing the structure of individual tree crowns, UAV imagery is ideally suited for this task. UAV imagery has been used in many different agricultural settings [14], but only to a limited extent for tree crops. For instance, measurements of plant height is a common UAV application because of the ability to produce photogrammetrically derived Digital Surface Models (DSM) from Structure-from-Motion of overlapping photos with different view angles of the same feature [4,19]. Plant height can be used to model biomass, which is crucial information for predicting crop yield [20-22].

Most UAV based tree crop mapping applications have focused on olive trees [4,19,23-25]. These studies, which all achieved high correlations between field and image derived structural parameters, focused on deriving chlorophyll and leaf area index using a six-band multi-spectral Tetracam [23], and map tree height, crown diameter, volume and area using RGB and multi-spectral imagery [4,19,24,25]. [4] used UAV based RGB imagery to map tree position, projected crown area, height and volume of olive trees before, after and one year after pruning. Tree crown structure was assessed for trees subjected to three different kinds of pruning techniques, i.e. mechanical, adapted and traditional. It was found that trees subjected to more aggressive pruning experienced much more subsequent vegetative development for the three studied pruning techniques.

In forestry applications, local maxima identification techniques have been used for identification in delineation of individual tree crowns [26-28], and these techniques have also been used successfully by [18] using UAV image data for assessing of tree height and crown diameter. Recently, segmentation approaches and geographic object-based image analysis (GEOBIA) of high spatial resolution imagery have become the preferred means for delineating individual tree crowns, due to the additional information available in the

Peer-reviewed version available at Remote Sens. 2018, 10, 854; doi:10.3390/rs10060854

classification/delineation process in terms of shape, context, class-related and multi-scale information [29-33]. Because of the suitability of object-based image analysis for information derivation from high spatial resolution imagery [34], several UAV based studies are now starting to incorporate GEOBIA into their image processing workflow [4,17,18,25,35-37]. [24] used an object-based supervised classification using the Classification and Regression Tree (CART) algorithm for delineating olive trees. [25] developed a simple object-based mapping approach based on thresholding olive tree crown DSM values in relation to neighbouring ground for tree crown delineation. The object-based mapping approach developed by [4] was based on that by [25]. This new approach heavily relied on the generated DSM for identifying the tree crown boundaries. However, as photogrammetrically point cloud generated DSMs often do not align perfectly with tree crown edges, as shown in this research, incorrect measurements of crown area and volume may be obtained if these edges are not adjusted based on spectral information. In addition, [4] reported that only 80% (512) of the trees within the orchard were correctly photo-reconstructed on the three image dates, which highlights the need to include spectral information as well in the object-based tree crown delineation process rather than heavily relying on the generated DSM.

There is scant literature on the use of UAVs for mapping the influence of pruning on tree crop structural development and change [4]. To expand upon this lack, this research paper explores a novel and innovative approach to assess changes in tree structure, i.e. tree crown perimeter, width, height, area and Plant Projective Cover (PPC), using multi-spectral UAV derived imagery collected before and after pruning. To do this, we focus our study on the analysis of a commercial lychee plantation in eastern Australia. An object-based tree crown delineation approach is introduced, representing an additional novelty that addresses limitations of other UAV based studies [e.g. 4,25]. Given the lack of any systematic evaluation of how UAV based data acquisition configurations, including varying flying heights, affect image derived information extraction of tree structure, a secondary objective was to assess any variations in the results as a function of various flying heights (30 m/4.1 cm pixels, 50 m/6.5 cm pixels and 70 m/8.8 cm pixels).

2. Study Area

The study was undertaken across a private lychee plantation located 25 km southeast of Brisbane, Australia (Figure 1). The lychee trees belong to the Kwai May Pink cultivar and were between 15 to 17 years of age, excluding 10 newly replanted trees. Each tree was planted approximately 4 m apart. The area has an elevation of 150 m above mean sea level and an average monthly mean temperature ranging from 15.1°C to 26.0° C, and an average annual rainfall of 1079 mm [38]. The orchard, consisting of 189 lychee trees, is surrounded by eucalypt forest.

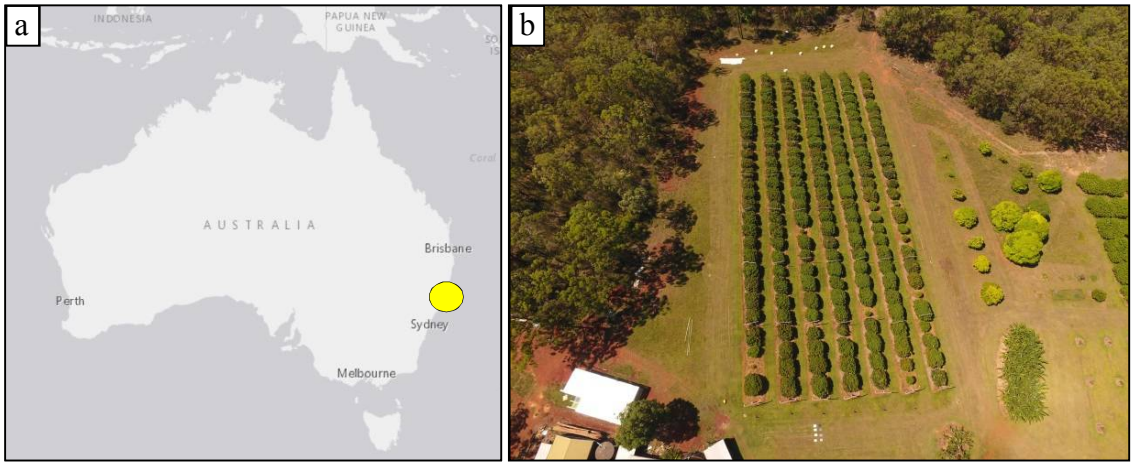

Preprints (www.preprints.org) | NOT PEER-REVIEWED | Posted: 16 April 2018 doi:10.20944/preprints201804.0198.v1

Peer-reviewed version available at Remote Sens. 2018, 10, 854; doi:10.3390/rs10060854

Figure 1. (a) Study area location (yellow dot) approximately 25 km southeast of Brisbane; (b) overview photo of study site; and (c) field photo of the lychee trees and poles used for protective nets to cover the trees.

3. Materials and Methods

3.1 Field Data

Field based measurements of tree height, crown width, crown perimeter and PPC from 89 out of the 189 lychee trees were collected on March 4th 2017. Tree height was measured as the distance from the ground to the top of the tree crown, using a retractable measuring staff. Crown perimeter was measured using a tape measure surrounding the widest part of the tree crown. Tree crown width was measured with a tape measure along the widest axis of each tree. For measuring PPC, four representative photos were taken underneath each of the 89 trees looking straight up. The photos were taken close to the ground and approximately half way between the tree trunk and the edge of the tree crown perimeter. These photos were analysed to determine PPC, i.e. the vertically projected fraction of leaves and branches in relation to sky. Measurements of PPC were derived using a program written in IDL® [39] to convert vertical digital photos to measurements of PPC based on the principle described by [40]. The derived PPC values of the four photos for each tree were then averaged to determine a representative PPC measure for each tree crown.

3.2 UAV Data and Pre-Processing

UAV multi-spectral (green: 530-570 nm; red: 640-680 nm; red edge: 730-740 nm; and Near Infrared (NIR): 770-810 nm) imagery was collected via a Parrot Sequoia sensor mounted to a 3DR Solo quadcopter for the lychee plantation on February 11th 2017 (pre-pruning) and March 4th 2017 (post-pruning). The Tower Beta Android application was used to autonomously collect imagery acquired with 80% sidelap and 85% forward overlap, at heights above ground level of 30, 50 and 70 m, producing 360, 278, and 202 photos per band, respectively.

The Parrot Sequoia imagery was processed in Pix4D Mapper to produce an orthomosaic, a DSM and a DTM for each of the six flights, i.e. two collection dates at three different heights. The DSM was created based on the generated point cloud and the inverse distance weighted interpolation method in Pix4D Mapper. The DTM was generated using the automatic function in Pix4D Mapper that uses the raster DSM and computes a classification mask of features above ground to generate a raster DTM based on ground features only. A canopy height model (CHM) was produced by subtracting the DTM from the DSM. The three flying heights produced orthomosaics with pixel sizes of approximately 4.1 cm, 6.5 cm and 8.8 cm, respectively.

To ensure an accurate georectification of retrieved imagery, 10 AeroPoints (i.e. Global Navigation Satellite System enabled ground control points, 54 cm x 54 cm x 3.5 cm in size, designed specifically for the geo-referencing of UAV imagery) were evenly spaced within the study area and used for geo-referencing of the imagery and for improving the Structure-from-Motion 3D model in Pix4D Mapper (Figure 2). These AeroPoint units are Global Navigation

Satellite System enabled ground control points, 54 cm x 54 cm x 3.5 cm in size, designed specifically for the geo-referencing of UAV imagery. The coordinate location of each AeroPoint was recorded for more than 3 hours, automatically uploaded after the flights using a mobile phone hotspot, and subsequently post-processed using the proprietary Propeller® Post Processed Kinematic network correction based on their nearest base station [41].

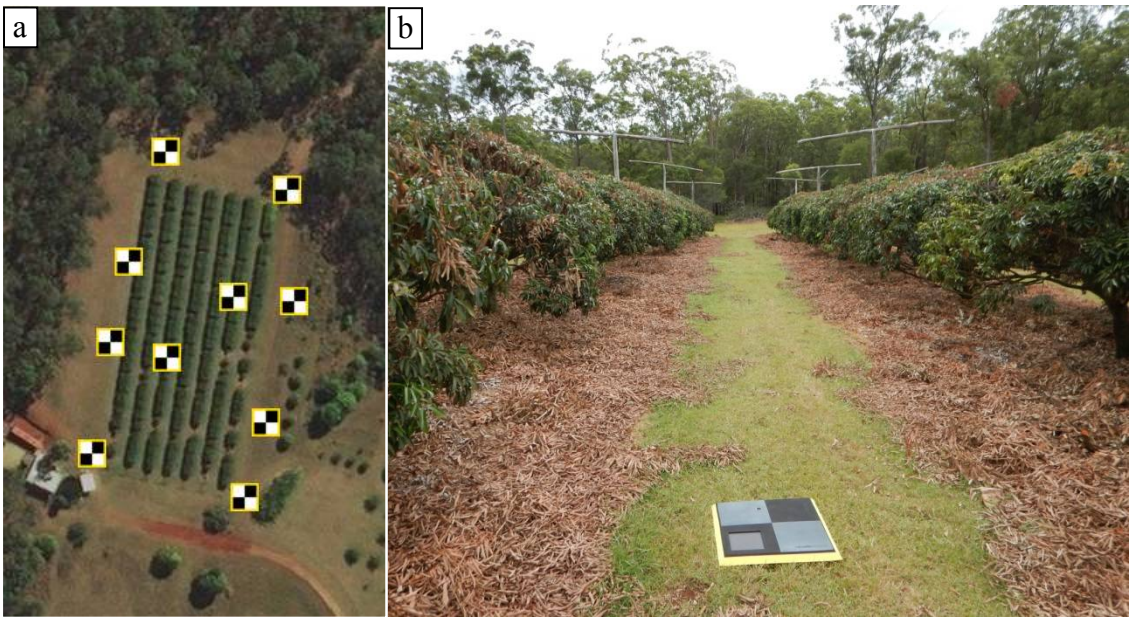

Figure 2. (a) Distribution and (b) in-situ field photo of AeroPoints used for geo-referencing of the UAV imagery.

Eight radiometric calibration targets were produced using Masonite boards painted with three coats of matt Dulux Wash and Wear paint in white, six scales of grey and in black [42]. The reflectance values of the eight targets were measured with an ASD FieldSpec 3 spectrometer (Figure 3) and confirmed to be near Lambertian. The RMSE of reflectance (scaled from 0-100%) ranged from 0.12% to 0.88%, between 500-850 nm, corresponding to the spectral range of the Parrot Sequoia sensor, based on spectrometer measurements obtained at 13 different angles, i.e. at nadir and at approximately 15°, 30° and 45°off-nadir angles viewed from north, south, east and west. Off-nadir view angles beyond 45° were not assessed, as the Parrot Sequoia sensor has vertical and horizontal field of views of 48.5° and 61.9°, respectively. Hence, the 45°off-nadir angle of the field spectrometer was well within the Parrot Sequoia sensor field of view, while still allowing for wind induced pitch, roll and yaw effects during each flight mission. Based on the relationship between the field derived spectrometer measurements, matched to each of the four spectral Parrot Sequoia bands, and the digital numbers of the eight radiometric calibration targets within the orthorectified multi-spectral imagery, the digital numbers were converted to at-surface reflectance using an empirical line correction in the ENVI 5.3 software [43].

Preprints (www.preprints.org) | NOT PEER-REVIEWED | Posted: 16 April 2018 doi:10.20944/preprints201804.0198.v1

Peer-reviewed version available at Remote Sens. 2018, 10, 854; doi:10.3390/rs10060854

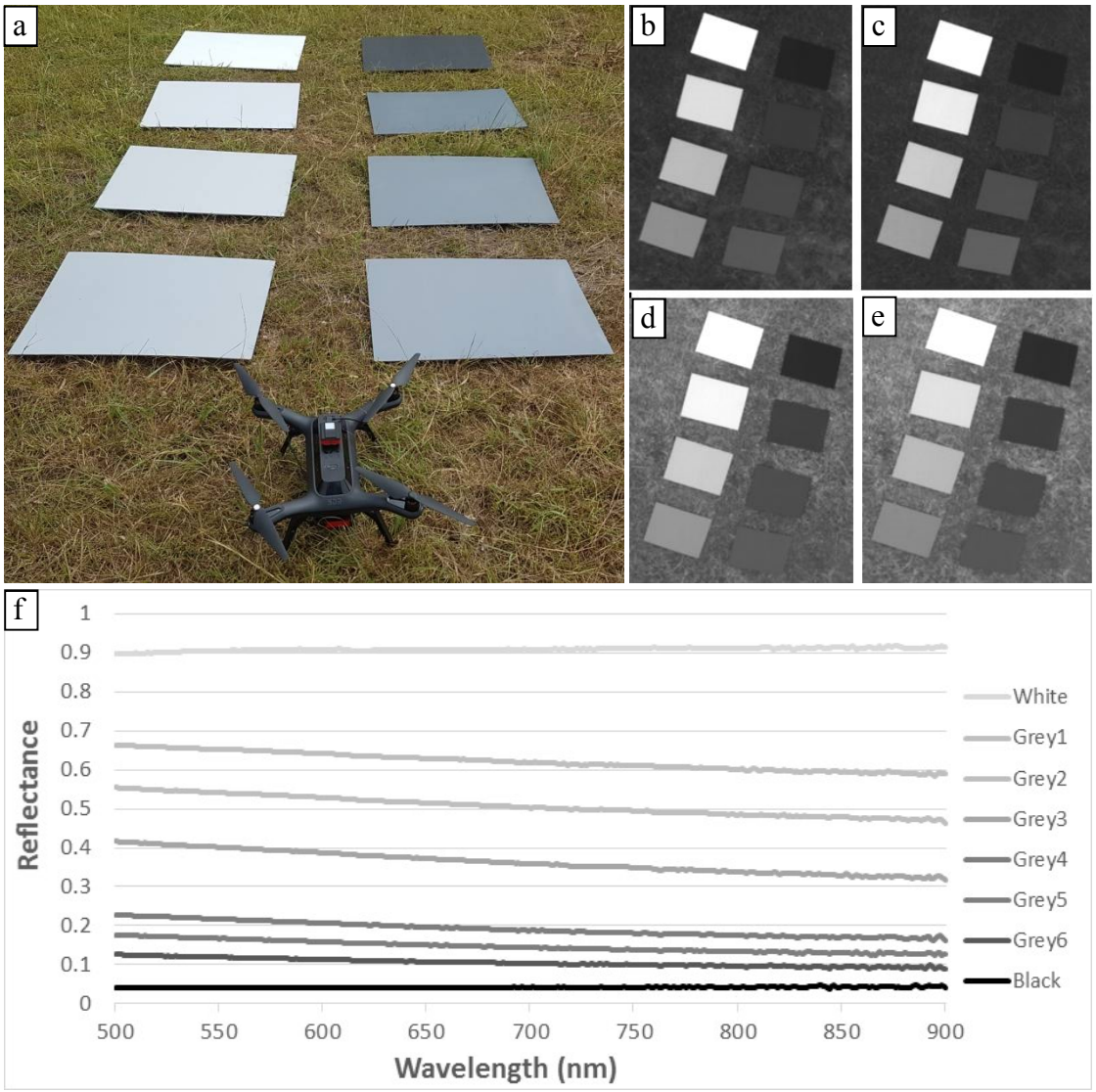

Figure 3. (a) Eight radiometric calibration targets and the 3DR Solo quadcopter; (b) green band; (c) red band; (d) red edge band; (e) NIR band; and (f) corresponding reflectance signatures between 500 and 900 nm of the eight targets.

3.3 Geographic Object-Based Image Analysis

GEOBIA and the eCognition Developer 9.2 software were used to automatically delineate the individual tree crowns based on the CHM and the multi-spectral orthomosaic. An object-based mapping approach was deemed most suitable because of the small pixel size in relation to the tree objects being mapped [34]. A detailed flowchart of the GEOBIA processing steps is presented in Figure 4. Tree crowns were initially identified for those areas in the CHM > 1 m. Tree crown objects were then grown outwards based on progressively lower CHM thresholds. The tree crown edges were adjusted based on spectral information. Once the tree crown extent had been mapped, the approximate tree crown centre of each tree was identified based on the CHM by searching for local maxima within the mapped tree extent. To avoid having multiple local maxima within a single tree crown, only the highest CHM value within a radius of 3 m was considered. Subsequently, these tree crown centres were grown outwards as long as the tree crown height decreased and until the length of each tree crown object reached 3 m. A mean filter was used to smooth the CHM for this region-growing step in order to avoid issues due to variations in tree crown height caused by irregular branches increasing tree height within parts of individual tree crowns [18,33].

Next, various class-related context information was used to refine the delineation of individual tree crowns. For example, in some cases single tall branches created local high points in the smoothed CHM, which made the region-growing algorithm grow around the local high points. In those cases, where excluded objects within the mapped tree extent were surrounded by objects classified as a single tree crown, these objects were then classified as part of the single tree crown. Also, edges of trees were expanded to include the full extent of the mapped tree extent without the requirement of having progressively lower CHM values. Unclassified objects appearing in between two neighbouring adjoining tree crows were assigned to a respective tree crown based on the width-length ratio of these individual tree crowns and the values of the filtered canopy extent mask. A tree crown having a smaller length-width ratio than its neighbouring and adjoining tree crown was allowed to grow into the remaining unclassified objects between the two tree crowns as long as the filtered canopy extent mask values of the unclassified objects were decreasing. Using the filtered canopy extent mask assumed that an indent in the canopy extent mask would occur between each adjoining tree crown (Figure 5). A looping function was used to progressively assess the width-length ratio of the neighbouring and adjoining tree crowns to increase the likelihood of objects being assigned to the tree crown they belonged to. These assumptions were not required for the post-pruned trees, as neighbouring tree crowns did not adjoin in most cases.

Preprints (www.preprints.org) | NOT PEER-REVIEWED | Posted: 16 April 2018 doi:10.20944/preprints201804.0198.v1

Peer-reviewed version available at Remote Sens. 2018, 10, 854; doi:10.3390/rs10060854

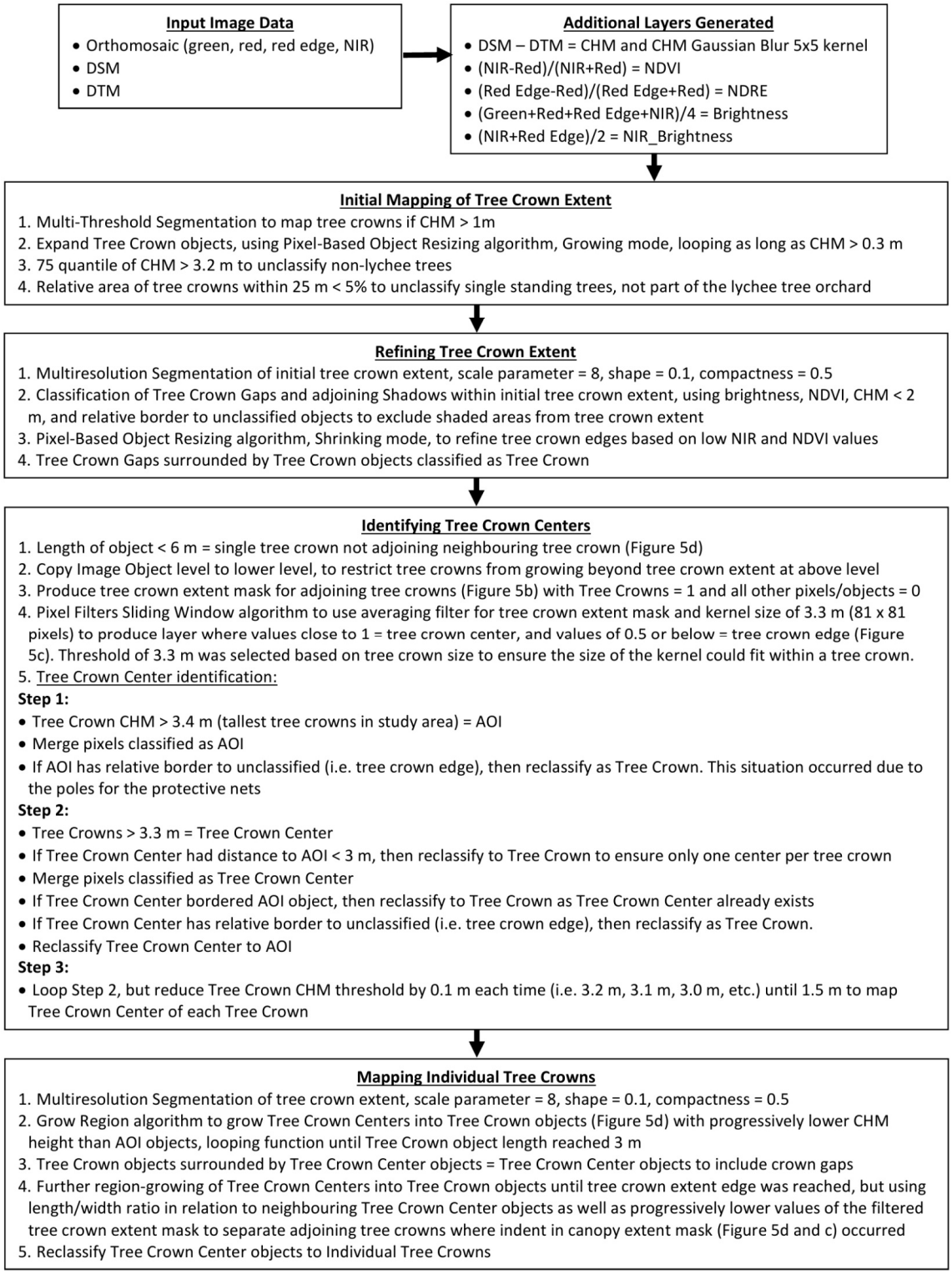

Figure 4. Flowchart of GEOBIA processing routine to map individual tree crowns.

Preprints (www.preprints.org) | NOT PEER-REVIEWED | Posted: 16 April 2018 doi:10.20944/preprints201804.0198.v1

Peer-reviewed version available at Remote Sens. 2018, 10, 854; doi:10.3390/rs10060854

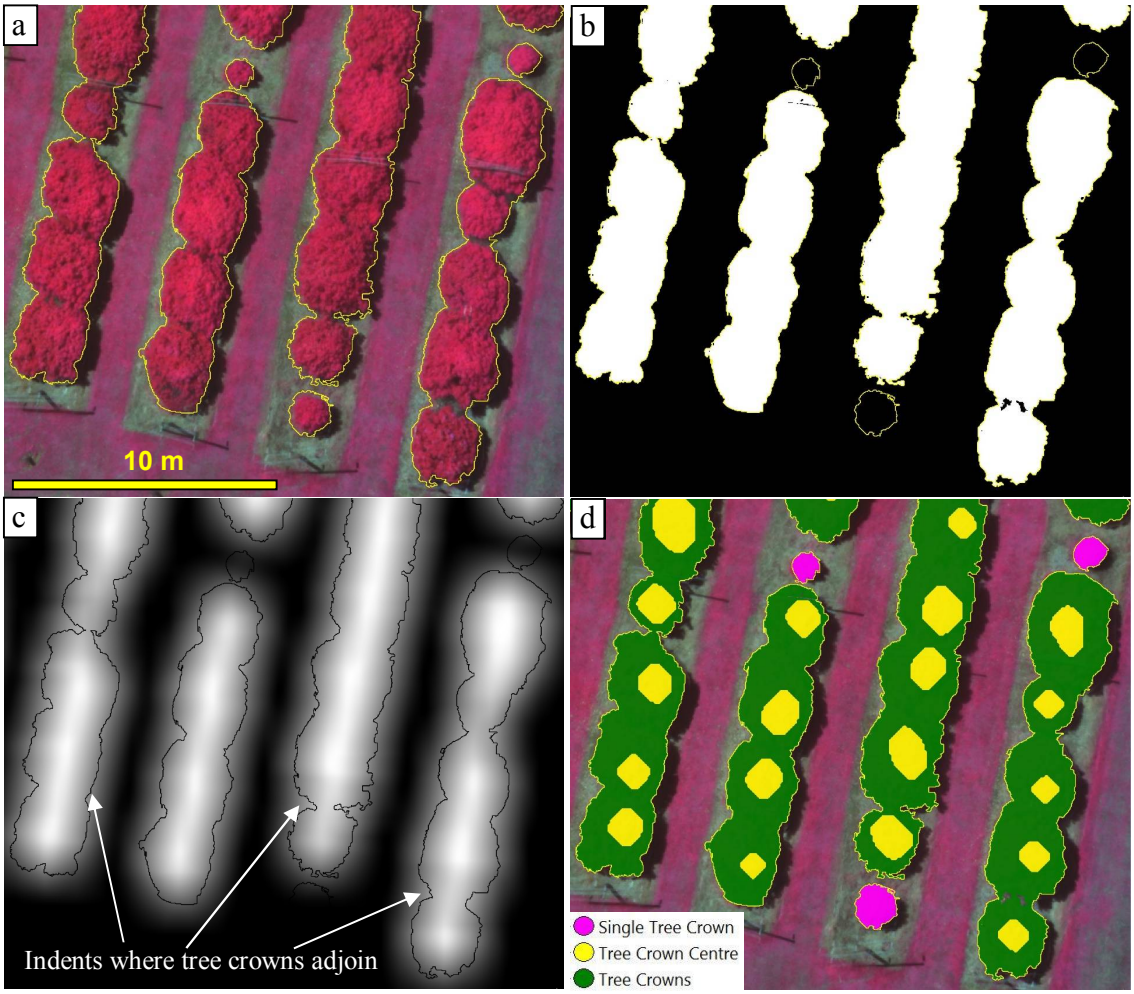

Figure 5. (a) False colour (Green, Red, NIR) image of pre-pruned lychee trees; (b) tree crown extent map; (c) tree crown extent map exposed to averaging filter with kernel size of 81 x 81 pixel; and (d) single tree crowns and tree crown centres being grown into tree crowns.

The 89 field assessed tree crowns, representing post-pruning condition, were manually delineated from the orthomosaic for validating the automatically delineated tree crown areas at the three different flying heights. The approach suggested by [44] and applied by [25] was used to assess the classification accuracy based on three classes, i.e. correctly mapped, omission error, and commission error in terms of object area.

3.4 Tree Crown Parameter Extraction

Based on the delineated tree crowns, a measure of their perimeter, area, width and height could automatically be derived in the eCognition Developer software. The image derived parameters were directly related to the corresponding field measurements of perimeter and tree crown width. However, tree crown area was not measured in the field, but was included for the assessment, comparing pre- and post-pruning structure. Although the maximum tree height was measured in the field, the 90th percentile of tree crown height was extracted at the individual tree crown object level to remove potential effects of the poles next to some of the trees, which are used for placing protective nets over the trees (Figure 1). These poles were taller than the trees and hence had to be removed from the image based estimates of height. Using the 90th percentile of tree crown height addressed this problem, and as the tree tops were fairly flat, it did not significantly lower the image derived tree height measurements.

The spectral bands, derived vegetation indices and co-occurrence texture measures were used to assess the correlation with the field photo derived PPC measurements. The spectral bands included the green, red, red edge and NIR bands. Derived vegetation indices included the NDVI, the Normalized Difference Red Edge Index (NDRE), the average brightness of all four spectral bands, and the average brightness of the red edge and NIR bands. Texture is the frequency of tonal change in an image. Second-order statistics derived from image spatial grey level co-occurrence matrix (GLCM) texture measures assume that information in an image is contained in the overall or average spatial relationship between pixel values (grey tones) [45-47]. The co-occurrence texture measures were calculated at the individual tree crown object level in the eCognition Developer software and included the Homogeneity, Contrast, Dissimilarity and Standard Deviation co-occurrence texture measures based on all four spectral bands [48]. All of these object variables were extracted for the 89 field assessed trees as a shapefile and combined with the field based measurements. PPC measurements were derived based on the best performing relationship with image extracted parameters for the post-pruned tree crowns. This relationship was used to convert the pre-pruning image into a map of PPC. For the comparison of pre- and post-pruning tree structure, the image derived maps with the optimal results in terms of flying height / pixel size were used, including all 189 mapped trees.

4. Results and Discussion

The results proved the importance of the tree crown delineation process, as this process enabled the extraction of tree structural parameters used to assess changes before and after pruning at the individual tree crown level. This also enabled an evaluation and comparison of the results derived from the UAV flights undertaken at three different flying heights.

4.1 Tree Crown Delineation

Since the derivation of tree structural parameters such as crown perimeter, area and width rely on the accuracy of the tree crown definition, the automated delineation of these using GEOBIA is a key step. As in other studies [4,18,22,25], the CHM was required for identifying individual tree crown centres and determining where the edges of two adjoining tree crowns were. However, in previous studies [25] adjoining tree crowns, forming a hedgerow has proven problematic to delineate. In this study, this problem was solved by using the length-width ratio of the tree crowns and the filtered tree crown extent mask, which were found to be essential for determining which objects, occurring between adjoining trees, belonged to which tree crowns. This was particularly the case for the pre-pruned tree crowns. Post-pruning, most of the tree crowns did not adjoin, and hence fewer assumptions had to be made to determine what objects belonged to each individual tree crown (Figure 6).

For tree crown delineations based on the imagery collected for the pre- and post-pruned lychee trees, all 189 lychee trees within the plantation were correctly identified. To achieve this accuracy, it was essential not only to rely on the CHM, but also to adjust tree crown edges based on the optical bands, as the tree crown borders often do not align with the DSM/CHM height information (Figure 7). Hence, while other eCognition Developer based approaches may have been computationally simpler to implement [4], such an approach would not have produced accurate results when applied to this research study. The accuracy assessment of the 89 manually delineated tree crowns investigated here showed that, on average, 98.6% of their area corresponded to that of the automatically delineated tree crowns, with an average error of omission of 1.4% and average error of commission of 2.2% (for the data set collected at 30 m flying height). The error of omission was reduced to 1.2% and 0.7%, while the error of commission increased to 2.4% and 3.1% for the data sets collected at 50 m and 70 m flying height, respectively. These results are well within reported tree crown delineation accuracies achieved using LiDAR data [49]. The slightly larger error of commission observed as a function of increased flying height

Preprints (www.preprints.org) | NOT PEER-REVIEWED | Posted: 16 April 2018 doi:10.20944/preprints201804.0198.v1

Peer-reviewed version available at Remote Sens. 2018, 10, 854; doi:10.3390/rs10060854

was attributed to the larger pixel size and how the corresponding DSMs were calculated, essentially resulting in the inclusion of an additional edge pixel surrounding the tree crowns with 8.8 cm pixels (70 m flying height) compared to the manually delineated tree crowns (Figure 6). This is a common characteristic when increasing the pixel size for tree crown delineation [28].

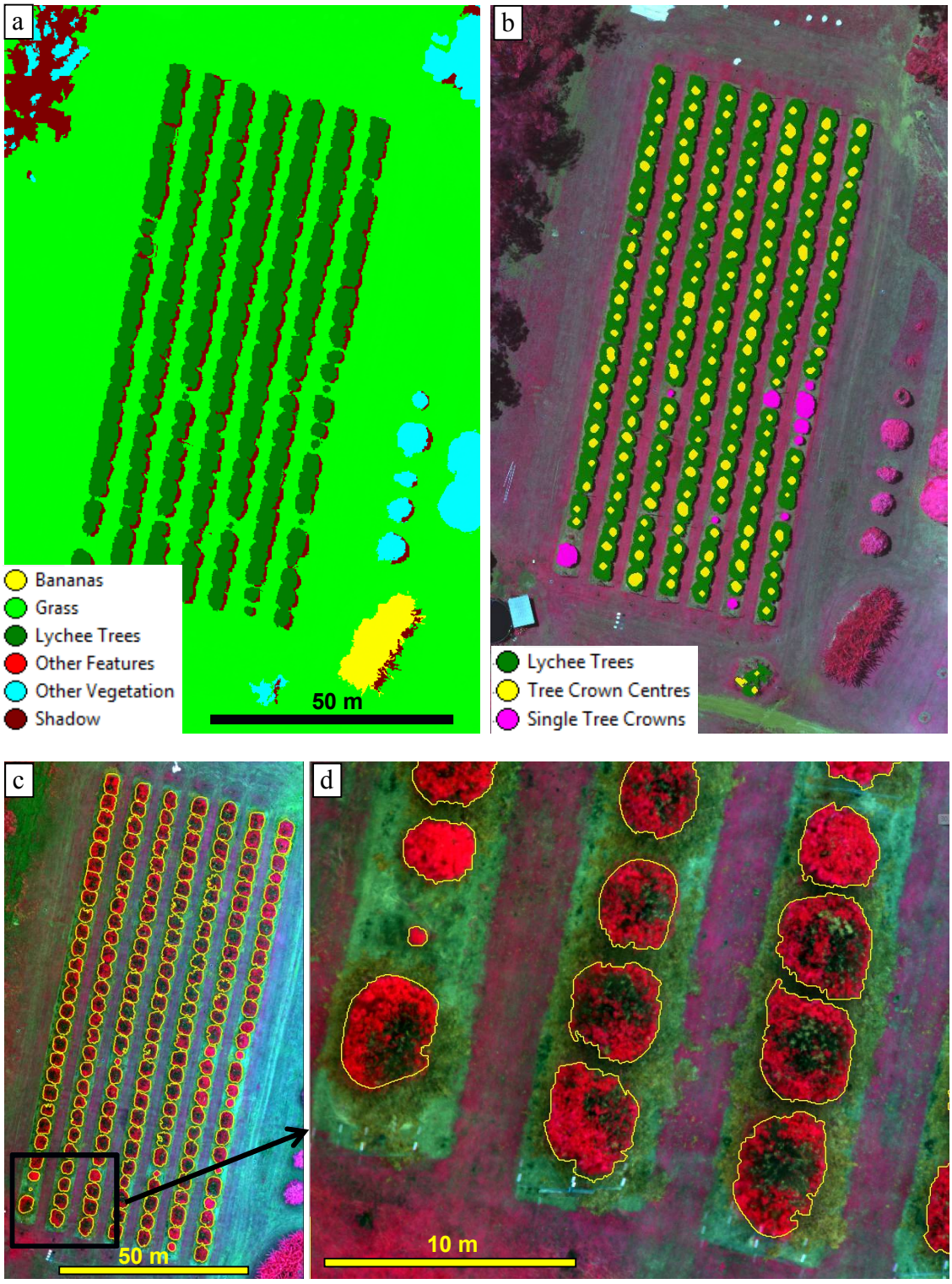

Figure 6. (a) Land-cover map, showing the mapped extent of pruned lychee trees; (b) identification of tree crown centres and single tree crowns not adjoining neighbouring tree crowns; (c-d) results of the lychee tree crown delineation (yellow outlines) produced using GEOBIA.

Preprints (www.preprints.org) | NOT PEER-REVIEWED | Posted: 16 April 2018 doi:10.20944/preprints201804.0198.v1

Peer-reviewed version available at Remote Sens. 2018, 10, 854; doi:10.3390/rs10060854

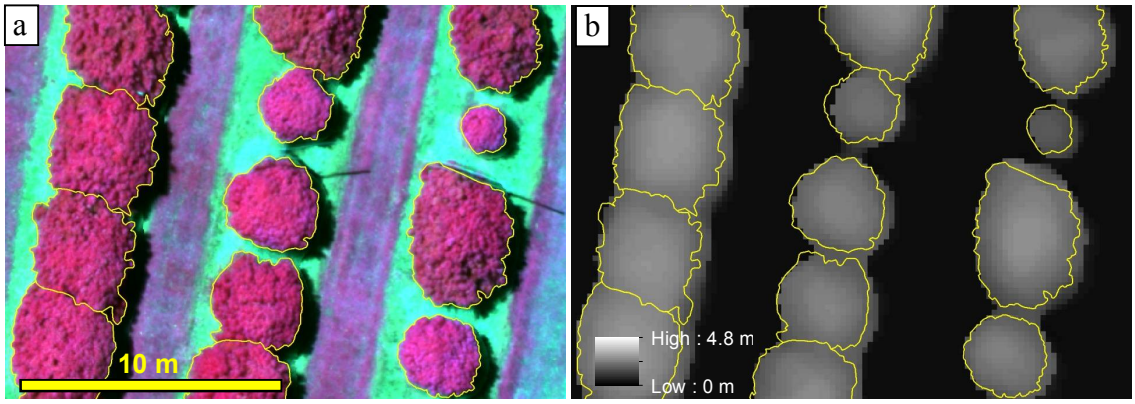

Figure 7. (a) False colour (NIR, Red, Green) orthomosaic; and (b) corresponding CHM of lychee trees post-pruning, including the GEOBIA delineation result (yellow outlines).

4.2 Mapping of Tree Structure

In addition to tree crown area, perimeter and width could be directly derived based on the delineated tree crowns. Tree crown perimeter measurements decreased slightly with increasing flying height due to the larger pixel size, producing a smoother crown edge delineation that was less affected by irregular branches along the tree crown edges. Flying at 70 m produced the highest R^2 value of 0.95 (n = 89) and the lowest RMSE of 3.42 m for mapping tree crown perimeter, as the smoothing of the tree crown delineation caused by the larger pixels corresponded to the way field based measurements of perimeter were obtained. Tree crown perimeter was overestimated in all cases and the RMSE varied from 3.42 m to 4.57 m. Although the larger pixel size of 8.8 cm (70 m flying height) produced a smoother outline of the tree crowns, corresponding to the way the field measurements were derived, an additional edge pixel surrounding the tree crowns with 8.8 cm pixels was still included, causing an overestimation of the perimeter (Figure 8). The different flying heights produced similar measurements of tree crown width with R^2 values of 0.90 - 0.93 (n = 89) and a RMSE of 0.62 - 0.65 m (Figure 8).

Preprints (www.preprints.org) | NOT PEER-REVIEWED | Posted: 16 April 2018 doi:10.20944/preprints201804.0198.v1

Peer-reviewed version available at Remote Sens. 2018, 10, 854; doi:10.3390/rs10060854

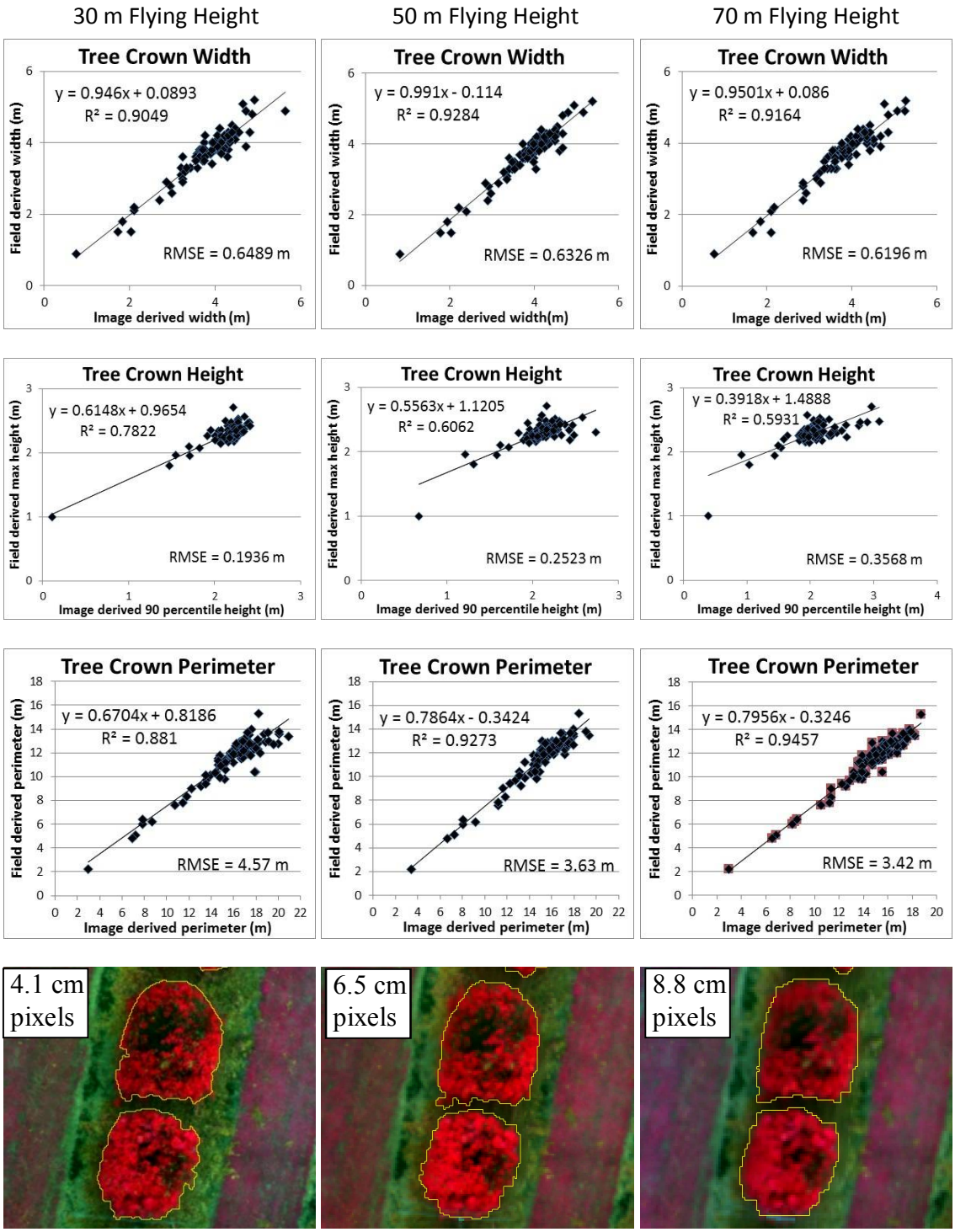

Figure 8. Relationships between field and image derived tree crown width, height and perimeter, and depiction of how the increasing pixel size affected the delineation of the pruned lychee tree crowns.

With increasing flying height, image derived measurements of tree crown height were increasingly underestimated. For the three CHMs produced at the three different flying heights, a less accurate DTM and an overall lowering of the DSM height of tree crowns occurred with increasing flying height. The highest R^2 value of 0.78 (with an RMSE of 0.19 m) was produced at a flying height of 30 m for estimating tree height. At flying heights of 50 and 70 m, the R^2 value

Peer-reviewed version available at Remote Sens. 2018, 10, 854; doi:10.3390/rs10060854

346 decreased to 0.61 and 0.59, with an RMSE of 0.25 m and 0.36 m, respectively (Figure 5). The
347 RMSEs are similar to those reported by [19, 25], who also assessed the effects of spatial resolution
348 on DSM generation and tree height quantification using UAV imagery, but for olive trees. In [19],
349 the tested pixel sizes were 5, 20, 25, 30, 35, 40, and 50 cm, and it was found that a significant
350 decrease in R^2 values and RMSE occurred at pixel sizes larger than 30 cm. However, those pixel
351 values were derived from resampling of UAV imagery collected at the same flying height as
352 opposed to our study where three different flying heights were used. A change of flying height
353 will affect the viewing geometry of the study area and hence the ability to reconstruct objects 3-
354 dimensionally. At lower flying heights, more extreme view angles of ground objects (in our case
355 lychee trees) are achieved, producing a larger parallax effect [50]. The reduced effect of parallax
356 at 70 m flying height may have caused the observed lowering of the DSM tree height. Also the
357 decrease in image spatial resolution with increased flying height may have caused local height
358 points, e.g. from single tree branches, to be missed in the point cloud generation used for the DSM
359 construction.

360 While different growing conditions, i.e. different lychee tree varieties, climatic conditions,
361 and pruning strategies, may influence the results and hence should be tested in future studies,
362 tree age and height are the main differences likely to be encountered between different orchards
363 in our particular study region. Ten of the lychee trees were younger and hence smaller than the
364 remaining 179 trees at this study site. Assessing only those 10 trees, it can be seen in Table 1 that
365 the RMSE of their height was higher than those in Figure 6, which was based on all 89 field
366 assessed trees. This indicates that the height for shorter and smaller trees were less accurately
367 mapped, and in all cases height was underestimated. This is similar to the findings of [25], where
368 underestimation of tree height occurred for shorter trees. Tree crown width and perimeter on the
369 other hand were mapped with significantly lower RMSE for the 10 younger trees. As these trees
370 were smaller and hence had a smaller perimeter, there was a shorter distance along which the
371 boundary line of the automatic tree crown delineation could appear irregular, due to branches
372 and other tree structural characteristics. This, and the absence of any adjoining tree crowns due
373 to the smaller crowns, also caused the width to be more accurately mapped. This indicates that
374 tree crown height may be less accurately mapped for younger and shorter trees, while tree crown
375 width and perimeter may in fact be mapped with higher accuracies for smaller trees.
376

377 Table 1. Root Mean Square Errors of mapped lychee tree crown height (90 percentile), width and
378 perimeter for the 10 youngest trees assessed against field data, post-pruning.

Flying Height (m)	Tree Height (m)	Crown Width (m)	Crown Perimeter (m)
30	0.3860	0.2280	2.5105
50	0.3934	0.2839	2.6700
70	0.6374	0.2604	2.3672

379

380 The highest R^2 values for estimating PPC were achieved using the red edge (R^2 = 0.79-0.81, n
381 = 89) and NIR (R^2 = 0.78-0.82, n = 89) bands, with the data collected at 70 m producing a slightly
382 higher positive correlation. The red band showed a poor correlation with PPC (R^2 = 0.04 - 0.15, n
383 = 89), due to little variation in red reflectance values in response to different PPC measurements.
384 Hence, spectral vegetation indices such as the NDVI and NDRE only produced R^2 values between
385 0.30 and 0.54. Using the co-occurrence texture measure of standard deviation of the red edge and
386 NIR bands, R^2 values between 0.57 and 0.70 were achieved (Figure 9). Co-occurrence texture
387 measures have been used successfully in other studies to assess vegetation structure and
388 measurements of PPC [48,51]. At the tree crown level, higher R^2 values for mapping PPC were
389 obtained in most cases for the imagery collected at 70 m height (8.8 cm pixels). In terms of the co-

Preprints (www.preprints.org) | NOT PEER-REVIEWED | Posted: 16 April 2018 doi:10.20944/preprints201804.0198.v1

Peer-reviewed version available at Remote Sens. 2018, 10, 854; doi:10.3390/rs10060854

occurrence texture measures, this may have been due to noise reduction caused by the larger pixel size, while the 8.8 cm pixel size still preserved useful within-tree crown texture information [52,53].

To estimate PPC of the pre-pruned tree crowns, for which no field data were collected, the best-fit equations between the post-pruned field derived PPC and the spectral bands, indices and texture measures were applied to the pre-pruned imagery to assess if these provided a realistic representation of PPC (Figure 10). The NIR band was found most useful for predicting PPC from the pre-pruning image, based on a visual assessment of the tree crowns and their within tree crown gaps. The NDVI showed little variation in estimated PPC, most likely because of saturation issues [54]. The use of the red edge band significantly overestimated PPC for many of the tree crowns. Using the texture measures for estimating PPC provided unrealistically large PPC variation and in many cases significantly underestimated PPC based on expectation (Figure 10).

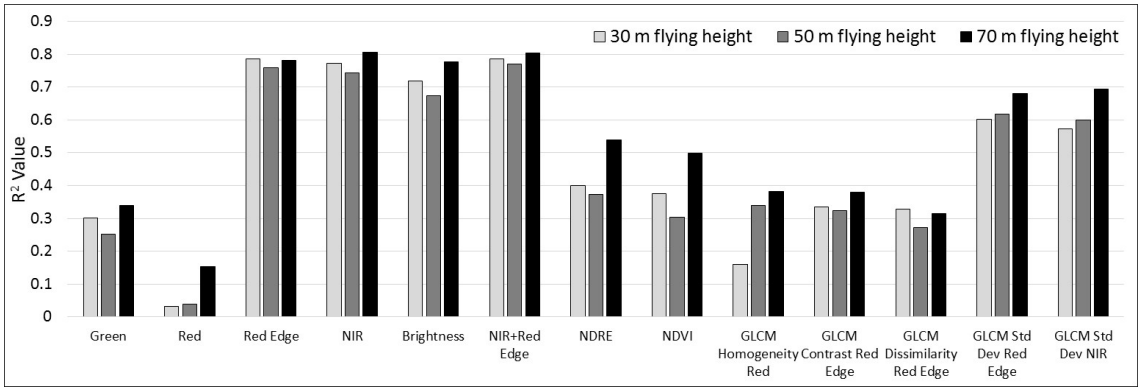

Figure 9. R^2 values based on the positive relationships between field measured PPC and image derived spectral bands, indices and texture measures produced from imagery collected at 30, 50 and 70 m flying height.

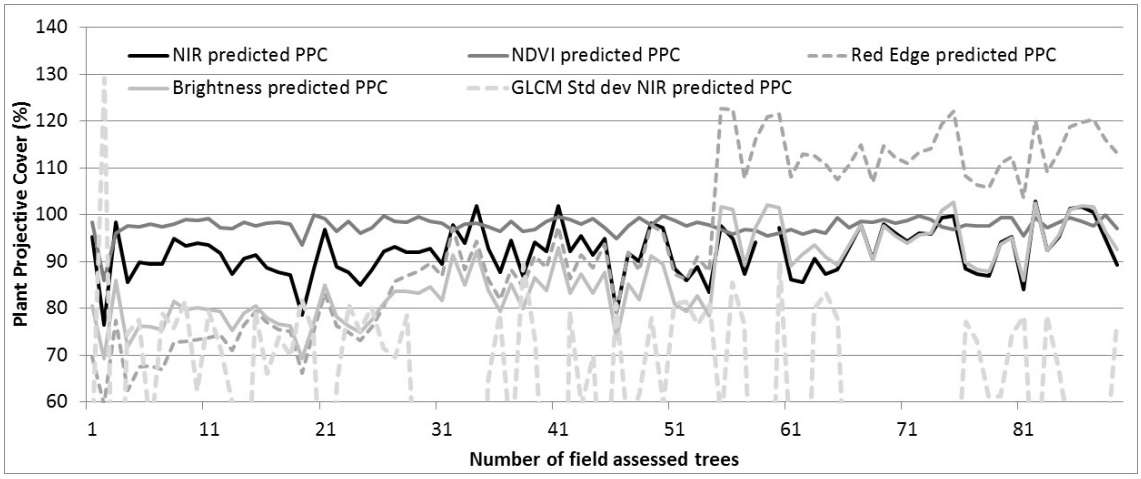

Figure 10. Estimated PPC of the 89 pre-pruned tree crowns for which PPC was measured post-pruning. PPC for the pre-pruned tree crowns was estimated using the best-fit equations based on the post-pruned image and field data.

4.3 Pre- and Post-Pruning Tree Structure Comparison

The mapping of tree structural parameters before and after pruning enabled an assessment of the impact of the pruning effects. A significant decrease in the average value of the tree structural parameters was observed for the 189 trees within the plantation between pre- and post-pruning. Decreases in the tree crown perimeter (1.94 m; 10.9%), area (3.49 m^2; 25.9%), width (0.567

Preprints (www.preprints.org) | NOT PEER-REVIEWED | Posted: 16 April 2018 doi:10.20944/preprints201804.0198.v1

Peer-reviewed version available at Remote Sens. 2018, 10, 854; doi:10.3390/rs10060854

m; 14.7%), 90th percentile tree crown height (0.616 m; 22.3%) and PPC (14.8%) were established (Figure 11). According to [12], the recommended thinning size of a lychee tree is between 15% - 25% from its initial size. Hence, the pruning results based on all 189 mapped trees showed good agreement with the recommendation. In most cases (179 out of 189 trees), a decrease was observed in the tree structural measurements for the individual tree crowns. However, some of the smaller and newly planted lychee trees (10 out of 189 trees) were not pruned, and hence the structural measurements stayed the same or slightly increased.

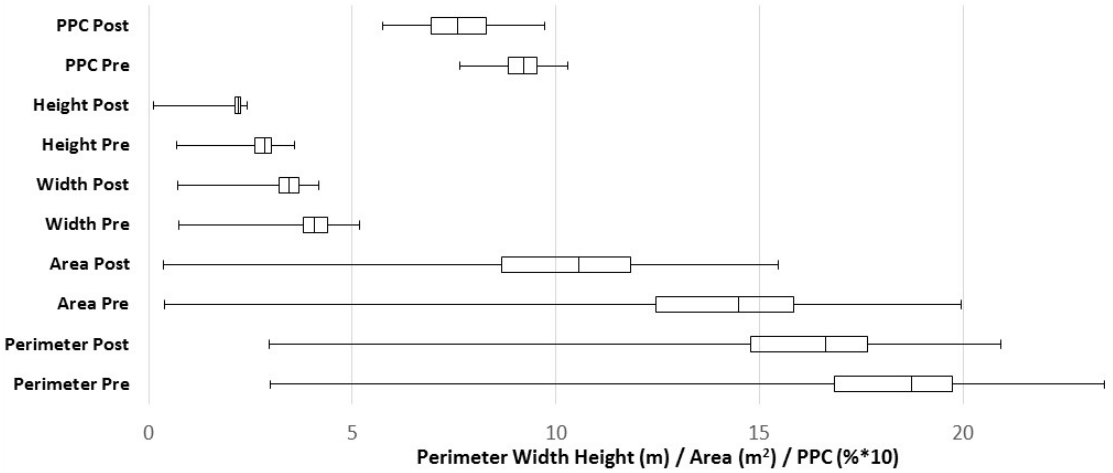

Figure 11. Pre- and post-pruning differences in minimum, Q1, median, Q3 and maximum values for the 189 mapped lychee trees for tree crown perimeter, area, width, 90th percentile height, and PPC measured from the UAV imagery collected at 30 m height.

4.4 Effects of Flying Height Differences

The impact of flying height variations offers insight into the influence of scale and the scalability of this UAV based approach to determine its applicability to larger orchards. Differences in flying height only affected the comparison of pre- and post-pruning tree structure slightly (Figure 12a). Tree crown height differences were highest when the imagery were collected at 30 m height compared to 50 and 70 m height. A flying height of 30 m produced the most accurate height estimates, given that the produced DSM and DTM were less accurate when collected at increasing flying heights. The measurements of area and perimeter decreased with increasing flying height because of the increasing pixel size, which made the automatically derived object perimeter smoother and hence smaller, despite the added tree crown edge pixels for the imagery collected at 70 m height that was discussed above. This also caused the differences in mapped area and perimeter to decrease as a function of flying height, because of the smaller range in values in these parameters at larger pixel sizes. The tree crown width measurements derived at different flying heights were similar, showing a slight decrease as the flying height (and hence the pixel size) increased, which also caused the differences before and after pruning to slightly decrease with increasing flying height (Figure 12a).

PPC was generally most accurately estimated based on the imagery collected at 70 m, although the average PPC difference was similar for all three flying heights (Figure 12b). However, at a flying height of 70 m, the average minimum and maximum differences were highest. Normally, at increasing pixel sizes, you would expect less spectral variability, i.e. a smaller range of pixel values within individual tree crown objects, because of spectral averaging of pixels covering a larger area [52]. This was attributed to the larger pixel size, which may have caused mixed pixels along the edges of the delineated tree crowns. These mixed pixels may have included parts of the shaded areas caused by tree shadows on the one side of the trees and parts of the sunlit green grass on the other side of some of the trees.

Preprints (www.preprints.org) | NOT PEER-REVIEWED | Posted: 16 April 2018 doi:10.20944/preprints201804.0198.v1

Peer-reviewed version available at Remote Sens. 2018, 10, 854; doi:10.3390/rs10060854

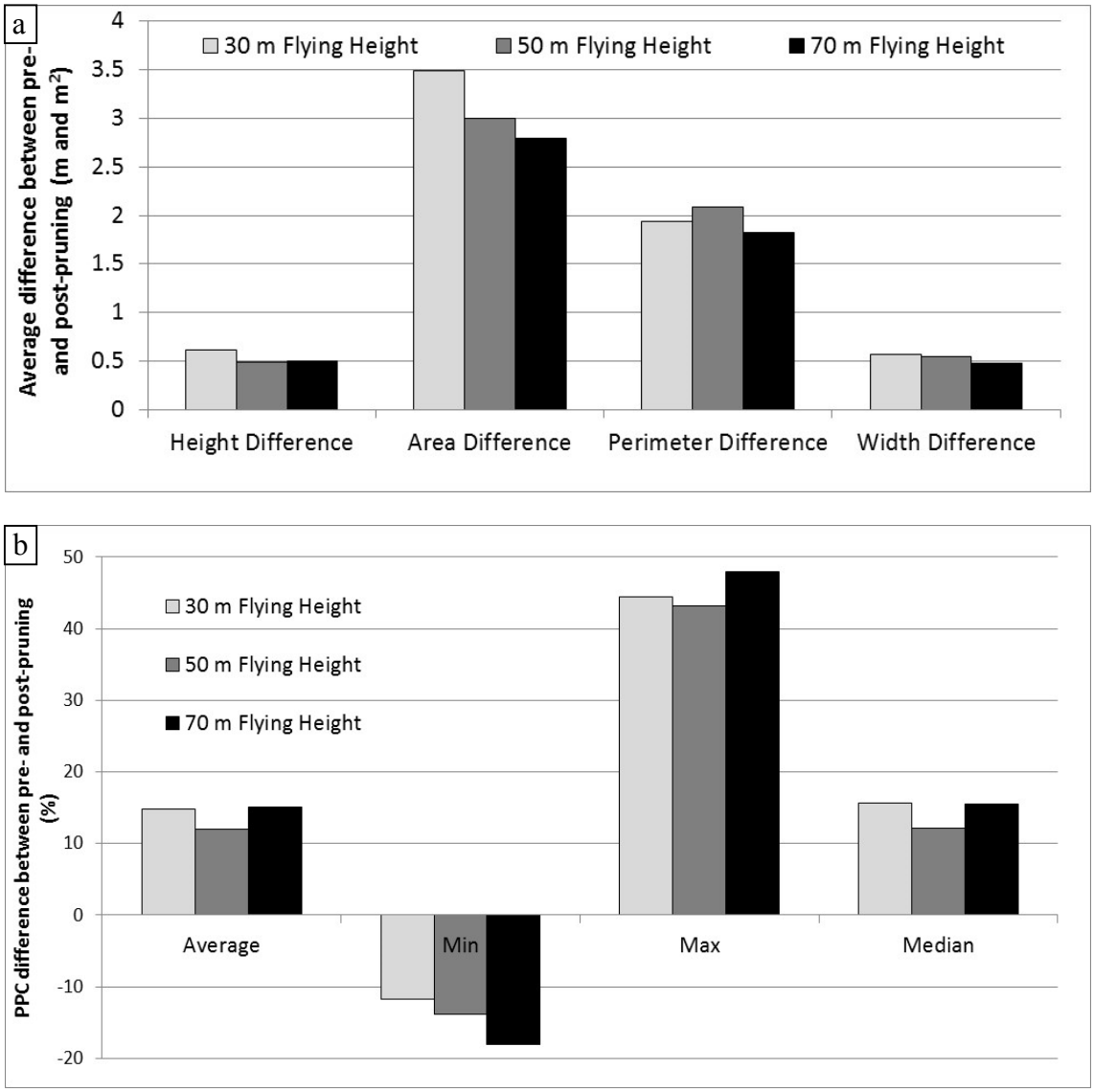

Figure 12. (a) Pre- and post-pruning differences for the 189 field assessed lychee trees for the 90th percentile tree crown height, area, perimeter, width; and (b) PPC, as a function of flying height.

There are clear management advantages to flying a UAV at a height of 70 m compared to 30 m, as it is possible to cover a larger area in a single flight or to reduce the flying time for covering a set area. Completing a flight mission more quickly also means that the risk to cloud shadow contamination is reduced. Although doing this resulted in an increase in pixel size from 4.1 cm to 8.8 cm and resulted in a compromise in tree height estimates using the Parrot Sequoia imagery, the mapping results of the vegetation structural parameters were not significantly affected. The acquisition of imagery with an 8.8 cm pixel size compared with 4.1 cm pixels will also reduce the size of the image data set more than fourfold, which will subsequently decrease the image processing time. [25] mapped tree structural parameters of olive trees from UAV imagery collected at 50 and 100 m above ground level and only observed small reductions in their predicted mapping accuracies, while significantly reducing the time of flight, the image orthomosaic processing and the GEOBIA, with total used time reduced from 47 min to 13 min and from 5 h 15 min to 1 h 8 min for their multi-spectral and RGB imagery, respectively. Hence, in terms of verifying the results of a pruning strategy on an orchard, there will likely be more efficiencies in choosing a flying height of 70 m, without loss of fidelity. Developing UAV based mapping and monitoring approaches for assessment of tree crop structure is also important for other types of tree crops, including mango, avocado and macadamia trees, as these parameters can provide information to help growers in the further production and delivery chain. This can ensure growers have enough personnel and equipment for fruit picking, have the right

478 storage facilities, have a suitable number of cartons for packaging, and can organise the means for transport
479 and delivery [55].

480 **5. Conclusions**

481 Characterizing the impacts of pruning on tree structural parameters is required to inform
482 and enhance the management of orchards and improve crop productivity. We present an
483 innovative and novel approach that exploits multi-spectral UAV imagery to measure tree
484 structural differences pre- and post-pruning, and apply this to a small commercial lychee
485 plantation. The developed object-based image analysis approach was found to be particularly
486 useful for delineating individual tree crowns and deriving object shape and spectral and textural
487 information for correlation with field based measurements of tree structure. The multi-spectral
488 imagery was found to accurately assess pre- and post-pruning tree crown structure, including
489 tree crown perimeter, area, width, height and PPC. Tree crown perimeter was most accurately
490 mapped at a flying height of 70 m, while tree crown width measurements were similar at all three
491 flying heights. Tree height was most accurately mapped at a 30 m flying height, as larger flying
492 heights affected the accuracy of the derived DSM and DTM. Imagery collected at 70 m height
493 produced slightly higher correlation with field measured PPC for most predictor variables.
494 These results highlight that despite the compromise in accuracy of tree height estimates
495 (0.1936 m RMSE as opposed to 0.3568 m), a flying height of 70 m may be the best choice for
496 assessing pre- and post-pruning tree structural differences to gain efficiency in terms of flight
497 duration, area coverage, and image processing time, without losing a significant amount of
498 information. As an additional benefit, the proposed UAV based approach is likely to reduce costs
499 (compared with manual assessment) and increase consistency compared to traditional field based
500 estimates. Future research should focus on collecting and analysing similar data for other orchard
501 sites and for trees grown under different conditions, e.g. different tree ages, tree varieties, climatic
502 conditions, and pruning strategies, to test if the developed approach can be applied more
503 generally and the results remain consistent with broader application.
504

505 **Acknowledgements:** This work was supported by the SPIRIT BAPPENAS-World Bank under Loan
506 Agreement (IBRD No. 8010-IND). Thanks to Paul Thorne, the lychee grower and owner of the lychee
507 plantation, for help in the field and for allowing us access to the study site. We would like to acknowledge
508 the Remote Sensing Research Centre in the School of Earth and Environmental Sciences at the University of
509 Queensland, Brisbane, Australia for use of software facilities. Matthew McCabe was supported by the King
510 Abdullah University of Science and Technology.

511 **Author Contributions:** Dr Johansen and Mr. Raharjo conceived and designed and performed the
512 experiments; Dr Johansen, Mr. Raharjo and Prof McCabe analyzed the data and wrote the paper.

513 **Conflicts of Interests:** The authors declare no conflict of interest.

514

515 **References**

516 1. Atzberger, C. Advances in remote sensing of agriculture: context description, existing operational
517 monitoring systems and major information needs. *Remote Sensing*, 2013, 949-981.
518
519 2. Me, C.Y., Balasundram, S.K., Hanif, A.H.M. Detecting and monitoring plant nutrient stress using remote
520 sensing approaches: a review. *Asian Journal of Plant Sciences*, 2017, 16: 1-8.
521
522 3. Ikinci, A. Influence of pre- and postharvest summer pruning on the growth, yield, fruit quality, and
523 carbohydrate content of early season peach cultivars. *The Scientific World Journal*, 2014, Article ID 104865, 8.
524

4. Jimenez-Brenes, F.M., Lopez-Granados, F., de Castro, A.I., Torres-Sanchez, J., Serrano, N., Pena, J.M. Quantifying pruning impacts on olive tree architecture and annual canopy growth by using UAV based 3D modelling. *Plant Methods*, 2017, 13, 55.

5. Rosell, J., Sanz, R. A review of methods and applications of the geometric characterization of tree crops in agricultural activities. *Computers and electronics in agriculture*, 2012, *81*, 124-141.

6. Sinoquet, H., Stephan, J., Sonohat, G., Lauri, P.É., Monney, P. Simple equations to estimate light interception by isolated trees from canopy structure features: Assessment with three-dimensional digitized apple trees. *New Phytologist*, 2007, *175*, 94-106.

7. Connor, D.J., Gomez del Campo, M., Rousseaux, M.C., Searles, P.S. Structure management and productivity of hedgerow olive orchards: a review. *Scientia Horticulturae*, 2014, 169, 71-93.

8. Menzel, C. Lychee production in Australia. In *Lychee production in the Asia-Pacific region*, 1st ed.; Papademetriou, M.K., Dent, F.J., Eds.; RAP Publication 2002/04. Food and Agriculture Organization of the United Nations, Regional Office for Asia and the Pacific, Bangkok, Thailand, March 2002.

9. Day, K.R., Dejong, T.M., Hewitt, A.A. Postharvest summer pruning of "Firebrite" nectarine trees. *HortScience*, 1989, 24, 238-240.

10. Miller, S.S. Regrowth, flowering and fruit quality of "delicious" apple trees as influenced by pruning treatments. *Journal of the American Society for Horticultural Science*, 1982, 107, 975-978.

11. Ferguson, L., Glozer, K., Crisosto, C., Rosa, U.A., Castro-Garcia, S., Fichtner, E.J., Guinard, J.X., Le, S.M., Krueger, W.H., Miles, J.A., Burns, J.K. Improving canopy contact olive harvester efficiency with mechanical pruning. *Acta Horticulturae*, 2012, 965, 83-87.

12. Campbell, T.P., Diczbalis, Y. *Pruning to meet your lychee goals: a report for the Rural Industries Research and Development Corporation*. Rural Industries Research and Development Corporation: Barton, A.C.T, Australia, 2001.

13. Lu, D., Mausel, P., Brondizio, E., Moran, E., 2004. Change detection techniques. *International Journal of Remote Sensing*, 2004, 25(12), 2365-2407.

14. Zhang, C., Kovacs, J. The application of small Unmanned Aerial Systems for precision agriculture: A review. *Precision Agriculture*, 2012, 13(6), 693-712.

15. Bagheri, N. Development of a high-resolution aerial remote-sensing system for precision agriculture. *International Journal of Remote Sensing*, 2017, 38(8-10), 2053-2065.

16. McCabe, M.F., Rodell, M., Alsdorf, D.E., Miralles, D.G., Uijlenjhoet, R., Wagner, W., Lucieer, A., Houborg, R., Verhoest, N.E.C., Franz, T.E., Shi, J., Gao, H., and Wood, E.F. The future of earth observation in hydrology. *Hydrology and Earth System Sciences*, 2017, 21, 3879-3914.

17. Kang, J., Wang, L., Chen, F., Nui, Z. Identifying tree crown areas in undulating eucaluptus plantations using JSEG multi-scale segmentation and unmanned aerial vehicle near-infrared imagery. *International Journal of Remote Sensing*, 2017, 38(8-10), 2296-2312.

18. Panagiotidis, D., Abdollahnejad, A., Surový, P., Chiteculo, V. Determining tree height and crown diameter from high-resolution UAV imagery. *International Journal of Remote Sensing*, 2017, 38(8-10), 2392-2410.

19. Zarco-Tejada, P.J., Diaz-Varela, R., Angileri, V., Loudjani, E. Tree height quantification using very high resolution imagery acquired from an unmanned aerial vehicle (UAV) and automatic 3D photo-reconstruction methods. *European Journal of Agronomy*, 2014, 55, 89-99.

20. Bendig, J., Yu, K., Aasen, H., Bolten, A., Bennertz, S., Broscheit, J., Gnyp, M.L., Bareth, G. Combining UAV-based plant height from crop surface models, visible, and near infrared vegetation indices for biomass monitoring in barley. *Geoinformation*, 2015, 38, 79-87.

21. Oerke, E.-C., Gerhards, R., Menz, G., Sikora, R.A. *Precision crop protection – the challenge and use of heterogeneity*. Springer: Dordrecht, Netherlands, 2010.

22. Matese, A., Di Gennaro, S.F., Berton, A. Assessment of a canopy height model (CHM) in a vineyard using UAV-based multispectral imaging. *International Journal of Remote Sensing*, 2017, 38(8-10), 2150-2160.

23. Berni, J.A.J., Zarco-Tejada, P.J., Suarez, L., Fereres, E. Thermal and narrowband multispectral remote sensing for vegetation monitoring from an unmanned aerial vehicle. *IEEE Transactions on Geoscience and Remote Sensing*, 2009, 47(3), 722-738.

24. Diaz-Varela, R.A., de la Rosa, R., Leon, L., Zarco-Tejada, P.J. High-resolution airborne UAV imagery to assess olive tree crown parameters using 3D photo reconstruction: application in breeding trials. *Remote Sensing*, 2015, 7(4), 4213-4232.

25. Torres-Sanchez, J., Lopez-Granados, F., Serrano, N., Arquero, O., Pena, J.M. High-throughput 3-D monitoring of agricultural-tree plantations with Unmanned Aerial Vehicle (UAV) technology. *PLOS ONE*, 2015, DOI: 10.1371/journal.pone.0130479.

26. Koch, B., Heyder, U., Weinacker, H. Detection of individual tree crowns in airborne Lidar data. *Photogrammetric Engineering and Remote Sensing*, 2006, 72(4), 357-363

27. Leckie, D., Gougeon, F., Hill, D., Quinn, R., Armstrong, L., Shreenan, R. Combined high-density lidar and multispectral imagery for individual tree crown analysis. *Canadian Journal of Remote Sensing*, 2003, 29(5), 633-649.

28. Pouliot, D.A., King, D.J., Bell, F.W., Pitt, D.G. Automated tree crown detection and delineation in high-resolution digital camera imagery of coniferous forest regeneration. *Remote Sensing of Environment*, 2002, 82(2-3), 322-334.

29. Bunting, P., Lucas, R. The delineation of tree crowns in Australian mixed species forests using hyperspectral Compact Airborne Spectrographic Imager (CASI) data. *Remote Sensing of Environment*, 2006, 101(2), 230-248.

30. Johansen, K., Bartolo, R., Phinn, S. Special Feature – Geographic object-based image analysis. *Journal of Spatial Science*, 2010, 55(1), 3-7.

31. Johansen, K., Sohlbach, M., Sullivan, B., Stringer, S., Peasley, D., Phinn, S. Mapping banana plants from high spatial resolution orthophotos to facilitate eradication of Banana Bunchy Top Virus. *Remote Sensing*, 2014, 6(9), 8261-8286.

32. Kamal, M., Phinn, S., Johansen, K. Object-based approach for multi-scale mangrove composition mapping using multi-resolution image datasets. *Remote Sensing*, 2015, 7(4), 4753-4783.

33. Kee, Y., Quackenbush, L.J. A review of methods for automatic individual tree-crown detection and delineation from passive remote sensing. *International Journal of Remote Sensing*, 2011, 32(17), 4725-4747.

34. Blaschke, T. Object Based Image Analysis for Remote Sensing. *ISPRS Journal of Photogrammetry and Remote Sensing*, 2010, 65, 2–16.

35. Laliberte, A.S., Herrick, J.E., Rango, A., Winters, C. Acquisition, orthorectification, and object-based classification of unmanned aerial vehicle (UAV) imagery for rangeland monitoring. *Photogrammetric Engineering and Remote Sensing*, 2010, 76(6), 611-672.

36. Ma, L., Cheng, L., Li, M., Liu, Y., Ma, X. Training set size, scale, and features in Geographic Object-Based Image Analysis of very high resolution unmanned aerial vehicle imagery. *ISPRS Journal of Photogrammetry and Remote Sensing*, 2015, 102, 14-27.

37. Torres-Sanchez, J., Lopez-Granados, F., Pena, J.M. An automatic object-based method for optimal thresholding in UAV images: Application for vegetation detection in herbaceous crops. *Computers and Electronics in Agriculture*, 2015, 114, 43-52.

38. Bureau of Meteorology, *Climate statistics for Australian locations*. URL: www.bom.gov.au/climate/averages/tables/cw_040854.shtml, (accessed on 19 March 2018).

39. Scarth, P. *A methodology for scaling biophysical models*. Ph.D. thesis. The University of Queensland, Brisbane, Australia, 2003.

40. van Gardingen, P.R., Jackson, G.E., Hernandez-Daumas, S., Russel, G., Sharp, L. Leaf area index estimates obtained for clumped canopies using hemispherical photography. *Agricultural and Forest Meteorology*, 1999, 94, pp. 243-257.

41. Propeller. *AeroPoints*. URL: https://www.propelleraero.com/aeropoints/, (last accessed 19 March 2018).

42. Wang, C., Myint, S.W. A simplified empirical line method of radiometric calibration for small Unmanned Aircraft Systems-based remote sensing. *IEEE Journal of Selected Topics in Applied Earth Observations and Remote Sensing*, 2015, 8(5), 1876-1885.

43. Ahmed, O.S., Shemrock, A., Chabot, D., Dillon, C., Williams, G., Wasson, R., Franklin, S.E. Hierarchical land cover and vegetation classification using multispectral data acquired from an unmanned aerial vehicle. *International Journal of Remote Sensing*, 2017, 38(8-10), 2037-2052.

44. Zhan, Q., Molenaar, M., Tem,pfli, K., Shi, W. Quality assessment for geo-spatial objectis derived from remotely sensed data. *International Journal of Remote Sensing*, 2005, 26(14): 2953-2974.

45. Franklin, S.E., Maudie, A.J., Lavigne, M.B. Using spatial co-occurrence texture to increase forest structure and species composition classification accuracy. *Photogrammetric Engineering and Remote Sensing*, 2001, 67, 849-855.

46. Haralick, R.M., Shanmugan, K., Dinstein, I. Textural features for image classification. *IEEE Transactions on Systems, Man, and Cybernetics*, 1973, 3(6), 610-621.

47. Clausi, D.A. An analysis of co-occurrence texture statistics as a function of grey level quantization. *Canadian Journal of Remote Sensing*, 2002, 28(1), 45-62.

48. Johansen, K., Coops, N.C., Gergel, S.E., Stange, Y. Application of high spatial resolution satellite imagery for riparian and forest ecosystem classification. *Remote Sensing of Environment*, 2007, 110(1), 29-44.

683 49. Kaartinen, H., Hyyppa, J., Yu, X., Vastaranta, M., Hyyppa, H., Kukko, A., Holopainen, M., Heipke, C.,
684 Hirschmugl, M., Morsdorf, F., Naesset, E., Pitkanen, J., Popescu, S., Solberg, S., Wolf, B.M., Wu, J.-C. An
685 international comparison of individual tree detection and extraction using airborne laser scanning. *Remote*
686 *Sensing*, 2012, 4, 950-974.
687
688 50. Lillesand, T., Kiefer, R.W., Chipman, J. *Remote sensing and image interpretation*, 7th Ed., Wiley, Hoboken,
689 USA, 2015.
690
691 51. Johansen, K., Phinn, S. Mapping structural parameters and species composition of riparian vegetation
692 using IKONOS and Landsat ETM+ data in Australian tropical savannahs. *Photogrammetric Engineering and*
693 *Remote Sensing*, 2006, 72(1), 71-80.
694
695 52. Puissant, A., Hirsch, J., Weber, C. The utility of texture analysis to improve per-pixel classification for
696 high to very high spatial resolution imagery. *International Journal of Remote Sensing*, 2005, 26(4), 733-745.
697
698 53. Woodcock, C.E., Strahler, A.H. The factor of scale in remote sensing. *Remote Sensing of Environment*,
699 1987, 21(3), 311-332.
700
701 54. Gu, Y., Wulie, B.K., Howard, D.M., Phuyal, K.P., Ji, L. NDVI saturation adjustment: A new approach
702 for improving cropland performance estimates in the Greater Platte River Basin, USA. *Ecological Indicators*,
703 2013, 30, 1-6.
704
705 55. Robson, A., Rahman, M.M., Muir, J. Using WorldView satellite imagery to map yield in avocado
706 (Persea Americana): A case study in Bundaberg, Australia. *Remote Sensing*, 2017, 9(12), 1223.